Available online at www.sciencedirect.com

ScienceDirect

Proceedings of the Combustion Institute 39 (2023) 73–84

Proceedings of the Combustion Institute

www.elsevier.com/locate/proci

New insights into the oxidation chemistry of pyrrole, an N-containing biomass tar component

Bingjie Chen [a], Peng Liu [b,*], Matteo Pelucchi [c,*], Clarissa Guidici [c], Luna Pratali Maffei [c], Sebastian Faller [a], Qiang Xu [d], Jiabin Huang [e], Feng Zhang [e], Can Huang [f], Kai Leonhard [f], Zhandong Wang [d,g], Marco Mehl [c], William L. Roberts [b], Tiziano Faravelli [c], Heinz Pitsch [a]

[a] *Institute for Combustion Technology, RWTH Aachen University, Templergraben 64, 52056 Aachen, Germany*
[b] *King Abdullah University of Science and Technology (KAUST), Clean Combustion Research Center, Thuwal, Saudi Arabia*
[c] *CRECK Modelling Lab, Department of Chemistry, Materials, and Chemical Engineering "Giulio Natta", Politecnico di Milano, Piazza Leonardo da Vinci 32, 20133 Milan, Italy*
[d] *National Synchrotron Radiation Laboratory, University of Science and Technology of China, Hefei, Anhui 230029, China*
[e] *Hefei National Laboratory for Physical Sciences at the Microscale, University of Science and Technology of China, Hefei, Anhui 230026, China*
[f] *Chair of Technical Thermodynamics, RWTH Aachen University, Schinkelstraße 8, 52062 Aachen, Germany*
[g] *State Key Laboratory of Fire Science, University of Science and Technology of China, Hefei, Anhui 230026, China*

Received 31 December 2021; accepted 3 July 2022
Available online 23 July 2022

Abstract

Pyrrole, the smallest molecule with a nitrogen atom in the heterocycle ring, is an important tar component from coal and nitrogen-rich biomass devolatilization. Understanding the combustion chemistry of pyrrole can help to elucidate the pollutant formation chemistry from fuel nitrogen, thus enabling cleaner biomass energy utilization technologies. Experimental measurements were performed in a jet stirred reactor coupled with time of flight molecular beam mass spectrometry using synchrotron vacuum ultraviolet beam as photon ionization source, and gas chromatography-mass spectrometry to provide comprehensive measurements of 31 species including nine C_4 and C_5 N-containing compounds. Based on the evidence from the experiments and aiming to improve the kinetic model performance, possible formation routes are proposed with OH addition as the entrance reaction. Reaction rate coefficients for the OH addition channel as well as those for key H-atom abstraction reactions (H, OH, CH_3, and HO_2) were calculated by quantum chemical methods and updated in the model. The updated model can qualitatively predict the identified C_4 N-containing species and perform reasonably well for a large set of experimental data considered for validation, overall improving

* Corresponding authors.
E-mail addresses: peng.liu.1@kaust.edu.sa (P. Liu), matteo.pelucchi@polimi.it (M. Pelucchi).

https://doi.org/10.1016/j.proci.2022.07.019

the performance of the previous model. The influence of the investigated reactions on the predictions of fuel reactivity and pollutant formation motivates further investigations of N-containing fuel chemistry.

Keywords: Pyrrole; N-containing species; Fuel nitrogen; H-atom abstraction; OH addition

1. Introduction

Biomass conversion by means of pyrolysis, gasification and combustion is a promising route for carbon-neutral energy supply [1]. However, burning biomass, especially protein-rich biomass, or conversion to bio-oils may elevate N-containing pollutant formation, e.g., NO_x from fuel nitrogen [2]. To achieve large-scale biomass utilization with low emissions and high efficiency, it is important to understand the pyrolysis and combustion chemistry as well as the fuel-NO_x pathways to assist advanced combustor design concepts [3].

Pyrrole (C_4H_5N) is an important component to represent the nitrogen content of tar from biomass devolatilization [4]. The molecular structure of pyrrole is interesting: the nitrogen atom is embedded in the five-membered unsaturated heterocycle ring. The unique chemical structure determines the reactivity and the tendency to form N-containing pollutants such as HCN and NO_x [5]. The pyrolysis of pyrrole was investigated by experiments [6–8] and theoretical studies [9–12]. The combustion chemistry was elucidated by ignition delay time measurements [13,14] and speciation in premixed flames [15], flow reactors [5,16], and jet stirred reactors (JSR) [17]. Pelucchi et al. [17] recently proposed the first comprehensively validated kinetic model. However, they found that a large amount of nitrogen was missing in the element balance of the speciation data in JSR oxidation. The missing nitrogen was assigned to the small N-containing species like NH_3 and NO_x that were not measured. Furthermore, the fuel reactivity at lean conditions (φ=0.5) was underpredicted by the kinetic model. These observations motivated this study towards a deeper understanding of pyrrole oxidation chemistry.

In this work, we apply advanced experimental techniques, and revisit pyrrole oxidation chemistry. The oxidation experiments were conducted in a JSR coupled with time of flight molecular beam mass spectrometry (ToF-MBMS) using synchrotron vacuum ultraviolet (SVUV) beam as photon ionization (PI) source and gas chromatography-mass spectrometry (GC–MS). Measurements of the N-containing species, including NH_3 and NO_x, were largely expanded. The proposed formation pathways for the identified C_4 N-containing species, and the calculated rates of H-atom abstraction and OH addition reactions were updated in the model, and it well predicts the experimental data. The importance of the investigated reactions was further substantiated with a wide range of model validations.

2. Methodology

2.1. JSR experiments

The JSR experiments were performed at the National Synchrotron Radiation Laboratory (NSRL), Hefei, China. Details of the measurement techniques are presented in previous literature [18], and specificities of this work are provided in the Supplementary Material (SM)−1. JSR conditions were: 1.05% fuel mole fraction, 2.0 seconds of residence time, equivalence ratio of 0.5, ambient pressure, argon as diluent, and temperature of 700–1050 K. The conditions are chosen to be similar to Pelucchi et al. [17] for data comparison, providing insights on the existing uncertainties in the experimental measurements and driving model improvement and reaction pathway exploration. The lean condition is chosen for investigation, because it shows the largest deviations between simulations and experiments [17].

Two experimental techniques were employed for speciation measurements. The first one is ToF-MBMS using SVUV as PI source, whose biggest principal advantage is to measure unstable radicals/intermediates and identify isomeric species. However, due to the relatively low concentrations, no radicals/unstable intermediates were measured. Therefore, we focused on the species identification performed by photon ionization efficiency (PIE) scans (8.00–10.50 eV, 0.05 eV/step, $T = 890$ K). Detailed data processing procedure can be found in [19], and the list of species ionization energies (IE) and photon ionization cross sections (PICS) is provided in Table S1 in SM-1. The estimated uncertainty is 20% for species with known PICS, and a factor of 2 for species whose PICS are calculated in this work. The second measurement technique is GC and GC–MS. Two GCs were used for measurements: Agilent GC1, equipped with a KCL Al_2O_3 capillary column and followed by a flame ionization detector (FID) to target measurements of small hydrocarbons except for formaldehyde, since its effective carbon number is zero, and a MolSieve 5a packed column followed by a thermal conductivity detector (TCD) for measurements of CO, CO_2, and H_2; Agilent GC-MS2, equipped with

an HP-5 capillary column followed by an FID and a mass-spectrometer detector (MSD) for measurements and identification of large hydrocarbon isomers based on the fragmentation information. The uncertainty of TCD in GC1 is estimated to be 20% for CO, CO_2 and H_2. For FID in GC-MS2, the uncertainty is estimated to be 10% for hydrocarbons [18]. Please note that the FID in GC1 may not be suitable for hydrocarbon measurements due to the low signals. The uncertainty for HCN is estimated to be 50% due to its low effective carbon number [20]. A summary of the detected species by ToF-MBMS, GC1, GC-MS2, and Pelucchi et al. [17] is listed in Table S2 in SM-1. The element balance is calculated by summing up the species mole fractions from different sources. More details on the element balance calculation are provided in SM-4. The total carbon recovery from the speciation data is above 90%. The nitrogen recovery is above 70% up to 950 K, but drops to 10% at 1040 K. Based on the model simulations discussed in Section 3.1, the missing N might be from N_2, HNCO, N_2O, and C_3HN that were not measured. Measurements of N-containing species could be enhanced by using Fourier-Transformed Infrared Spectroscopy, or a nitrogen phosphorus detector coupled with GC or GC–MS.

2.2. IE and pics calculations

IE of 28 possible structures for the detected chemical compositions (C_4H_3NO, C_4H_5NO, $C_4H_3NO_2$, C_5H_7N, C_5H_5NO, and C_5H_7NO) are calculated by various methods, e.g., m06–2x/aug-cc-pVTZ, m06-l/aug-cc-pVTZ, ROCBS-QB3, and G4 since the calculations failed with some of the methods. Details about the IE calculations and the uncertainties can be found in SM-1. Fig. S1 and Table S3 in SM-1 present the target molecular structures and the IE calculation results.

The PICSs of 6 N-containing species, namely propenenitrile, methanimine, acetonitrile, vinylamine, formamide, and 2-propen-1-amine, are theoretically predicted by the product of Franck-Condon envelope and transition moment [21,22]. Details of the method and the uncertainty are included in SM-1. The calculated PICS (Fig. S2 in SM-1) support the species quantification of ToF-MBMS measurements.

2.3. Reaction rate calculations

Reaction rate coefficients of H-atom abstraction reactions from pyrrole by OH, H, CH_3, HO_2 and OH addition were evaluated at the CCSD(T)/CBS//m06–2x/6–311+g(d,p) level of theory [23–25]. The automated tool EStokTP [26], which is coupled to the MESS master equation solver by Georgievskii et al. [27], was used for electronic structure calculations and master equation simulations. Thermodynamic properties for intermediate species in the updated model were calculated using the automated routines in [28]. SM-1 reports details about the calculation methods, potential energy surfaces (Figs. S3-S6), species nomenclature (Table S4), rate coefficients (Table S5), and thermodynamic properties (Table S6). Master equation [27] input files are included in SM-2 to ensure the replicability of the results. The rate comparison is presented in Figs. S7-S8 in SM-1.

2.4. Kinetic modeling

A kinetic model for pyrrole was recently proposed by Pelucchi et al. [17] and is here referred to as the CRECK model. The calculated rate coefficients are tentatively updated, and the obtained model is referred to as the updated model. Based on the experiments and theoretical calculations, the lumped CRECK model was partly delumped to distinguish the two radicals from H-atom abstraction of pyrrole: the resonance-stabilized pyrrolyl radical (PYRLYL) and one single C_4H_4N radical representing both the radical located in the alpha position to the nitrogen atom and that located in the beta position. This assumption is justified by the similar calculated bond dissociation energies (BDE) of C–H bond (BDE=118 kcal/mol) compared to the much lower BDE of the N–H bond (93.3 kcal/mol). BDEs are determined as part of the theoretical analysis for rate constant calculations. For OH addition on the C_4H_4N radical at alpha or beta site, we assume that there is little difference in the reaction rates. This is because the proximity of NH functional group is not expected to have major effects, as shown in the complete PESs of R+pyrrole in Figure S3–6 in SM-1 and the rigorous approach in the literature [29]. The updated model with thermodynamic properties is included in SM-3. The Chemkin Pro software [30] and OpenSMOKE++ [31] were used for simulations. Model comparisons with a wide range of validation targets is reported in SM-1.

3. Results and discussions

3.1. Speciation pool for quantified species

For the species that are identified and quantified, Figs. 1, 2, and 4 present the measured mole fractions versus temperature from different experimental techniques, kinetic model simulations, and the literature [17]. The blue circles are from ToF-MBMS using SVUV as PI source; yellow squares from GC1; olive triangles from GC-MS2; the red crosses from Pelucchi et al. [17]. Red dashed lines show results from simulations using the original CRECK model [17] while the black solid lines show the results from the updated model. The shaded areas with different colors indicate the uncertainties

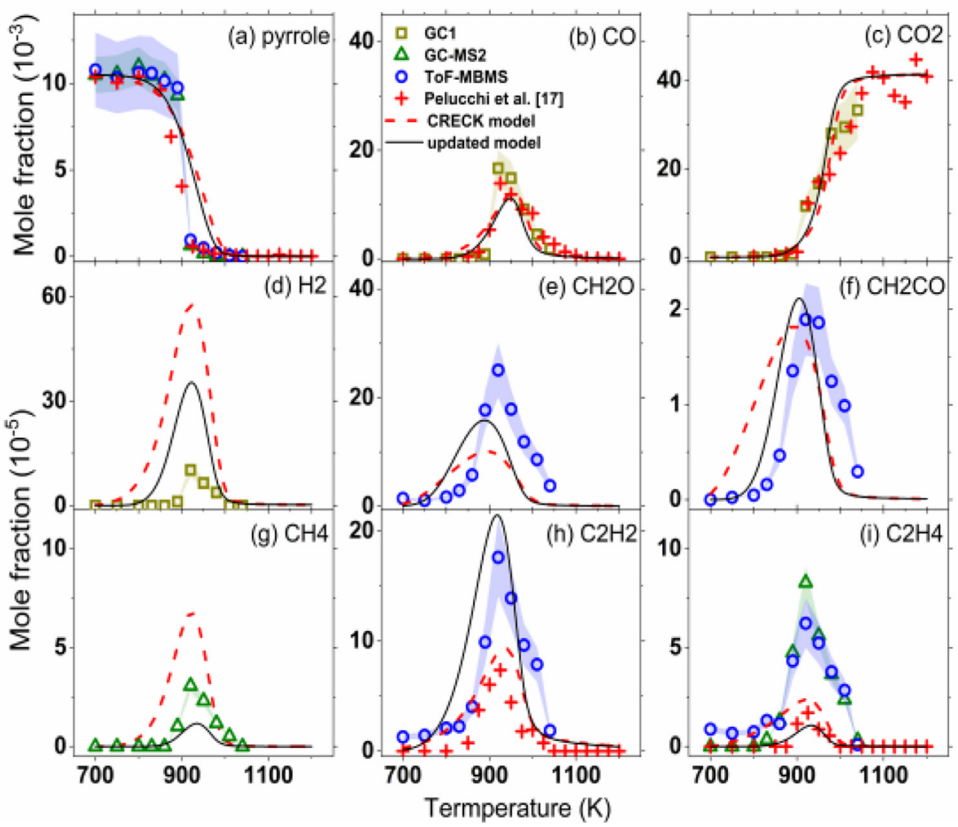

Fig. 1. Mole fraction versus temperature profiles of the reactants, main products, and small hydrocarbon intermediates. JSR conditions: fuel concentration 1.05%, φ=0.5, p = 1 bar, τ=2.0 s. The red crosses represent the experimental data from Pelucchi et al. [17].

of different experimental techniques. All the experimental data are provided in SM-4.

Fig. 1 shows the mole fraction versus temperature profiles of pyrrole, main products (CO and CO_2), and important intermediates (H_2, CH_2O, CH_4, C_2H_2, C_2H_4, and CH_2CO). The mole fraction of oxygen is presented in Fig. S9 in SM-1. The experimental datasets from different techniques and Pelucchi et al. [17] agree well for CO (Fig. 1(b)) and CO_2 (Fig. 1(c)). For pyrrole, some discrepancies appear between the measurements in this work and the datasets from Pelucchi et al. [17] around 900 K. The deviation might be caused by the temperature uncertainty since pyrrole consumption around 900 K is very sensitive to the temperature. Datasets of CH_4, C_2H_2, and C_2H_4 from GC1 are not presented due to low signal intensity. For acetylene, the ToF-MBMS measurements show higher values than the datasets from Pelucchi et al. [17], and have better agreement with the updated model prediction. For ethylene, both datasets from GC-MS2 and ToF-MBMS agree with each other and show higher values than datasets from Pelucchi et al. [17], which might require further investigations. In general, the good agreement among datasets from different experimental techniques provides a useful cross-validation and relevant indications for model refinement and assessment.

Concerning the model performance, the original CRECK model under-predicts the consumption of pyrrole between 900 and 1000 K (Fig. 1(a)). CO, CO_2, CH_2O, CH_2CO, C_2H_2, and C_2H_4 are well predicted, while H_2 (Fig. 1(d)) and CH_4 (Fig. 1(g)) are over-predicted. Sensitivity analysis for the original CRECK model at 900 K (see Fig. S10 in SM-1) indicates that, except for small molecule reactions, the H-atom abstraction reactions are the most sensitive reactions for pyrrole consumption. This motivated further investigations on the rate coefficients of H-atom abstraction reactions by predominant radicals like H, OH, HO_2, and CH_3, which have been already highlighted for their importance in pyrolysis, oxidation, and ignition delay time [17]. The availability of unsaturated bonds for OH addition reactions was not considered by Pelucchi et al. [17], so it was investigated in this work to improve the fuel consumption in the relatively low-temperature regime. Details of the

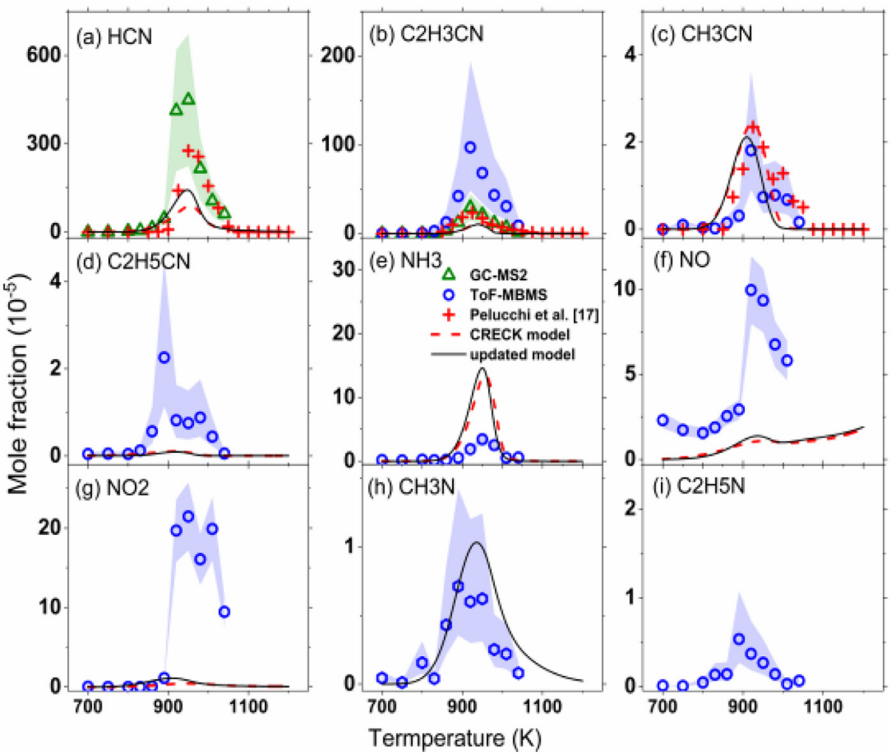

Fig. 2. Mole fraction versus temperature profiles of quantified small N-containing intermediates. JSR conditions: fuel concentration 1.05%, φ=0.5, p = 1 bar, τ=2.0 s. The red cross data is taken from Pelucchi et al. [17].

theoretical calculation methods and results are reported in SM-1. The updated model slightly improves the fuel conversion. In particular, the onset of pyrrole consumption is delayed by ~50 K compared to the original CRECK model and closer to the experiments. At T = 950 K, the predicted fuel consumption increases by 10% providing an overall better match with the experiments. CH_4 is now under-predicted by the updated model, which was over-predicted by the original model. In Fig. 1d, the over-prediction of H_2 is attenuated by the updated model, although it is still over-predicted. Predictions of C_2H_2 by the updated model agree better with the dataset from ToF-MBMS. Some discrepancies emerge for C_2H_4 predictions, which agree well with the measurements of Pelucchi et al. [17], but underestimate the data from this work.

Fig. 2 presents the mole fraction versus temperature profiles of nine representative small N-containing species: NH_3, NO, NO_2, HCN, CH_3N (methanimine), CH_3CN (acetonitrile), C_2H_3CN (propenenitrile), C_2H_5N (vinylamine), C_2H_5CN (propanenitrile). Many of these species, except for HCN, CH_3CN and C_2H_3CN, were not measured in the previous study [17]. The abundant N-containing species pool has direct implications on the N-containing pollutant formation from pyrrole.

The datasets of HCN, CH_3CN, and C_2H_3CN match well except for the C_2H_3CN data from ToF-MBMS. Since the uncertainty of ToF-MBMS measurements is higher than GC-MS2, we believe that the datasets of C_2H_3CN from GC-MS2 are more reliable. The datasets from GC-MS2 also agree with the datasets from literature [17]. For HCN, GC-MS2 measurements have high uncertainty due to the low effective carbon number, so the datasets from the literature [17] might be more trustable. However, multiple datasets may have greater value than single one even when the datasets differ. For model validation, one should take all datasets with the uncertainty into consideration and perform a statistical evaluation of the resulting model uncertainties [32]. Although the updated model slightly improves the predictions of HCN, both HCN and C_2H_3CN are still underpredicted, while CH_3CN is well predicted by both models. C_2H_5CN is underpredicted by over two orders of magnitude. Both models overestimate NH_3 by a factor of 3. Future work is needed to improve the N–C chemistry.

Both models underestimate the peak values of NO and NO_2 by up to one order of magnitude, representing one of the largest shortcoming of the kinetic model. A rate of production analysis on NO and NO_2 formation pathways is reported

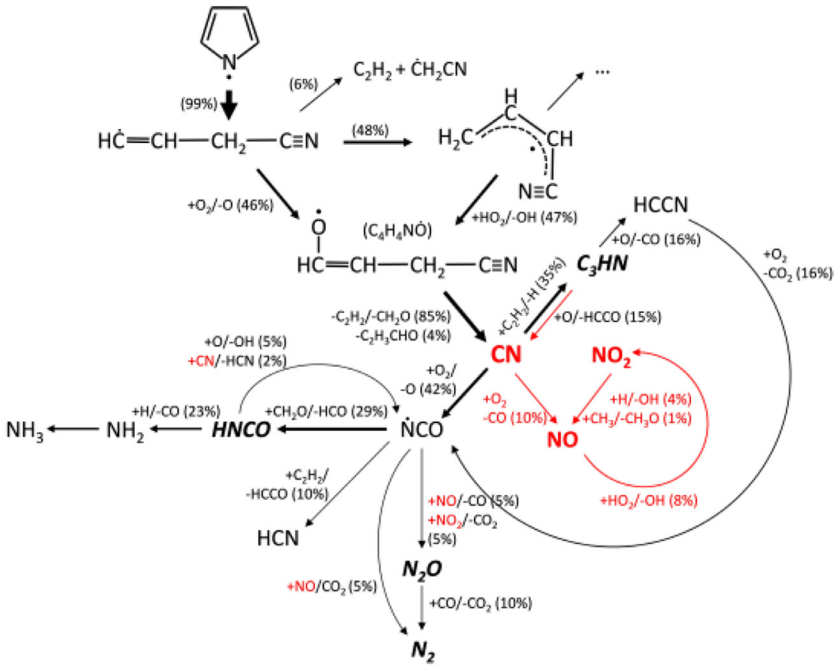

Fig. 3. Rate of production analysis of the updated model at $T = 925$ K, φ=0.5, $p = 1$ bar, τ=2.0 s highlighting the main NO and NO_2 formation pathways. Species in bold italics are abundant species (Fig. S12, SM-1) according to model predictions that are not experimentally measured.

in Fig. 3 to highlight possible sources of such deviations. The cyano radical (CN) is the major source of NO formation through the reaction CN+O_2⇌CO+NO, and it is mainly produced by the decomposition of allyloxy cyanide (C_4H_4NO) [17]. This reaction competes with CN radical addition to acetylene producing cyanoacetylene (C_3HN) and H atom. Results from a sensitivity analysis (Figure S22 in SM-1) highlight the key role of the relative branching ratio between CN+O_2⇌CO+NO and CN+O_2⇌O+NCO, with the former having a promoting effect and the latter an inhibiting effect on NO formation. The rate coefficients for the former reaction, which is highlighted also as sensitive for pyrrole consumption in Fig. S11 of SM-1, are adopted from Baulch et al. [33] with the branching fraction between the two channels as reported by Glarborg et al. [2] (i.e. 20/80 for CO+NO/ O+NCO). The beneficial effect of a 50/50 branching ratio is reported in Figure S23, pointing at the need of further revisiting the relative weight of CN+O_2 product channels. The rate coefficients of CN addition to acetylene are instead estimated by analogy with H-atom addition to acetylene [17]. C_3HN is one of the unmeasured nitrogenated compound that is formed in large quantities by model simulations. Specifically, the model predicts a peak of ~320 ppm at $T = 925$ K, as reported in Fig. S12 of SM-1. An equivalent flux of CN radical reacting with molecular oxygen yields isocyanate radical (NCO). NCO undergoes H-atom abstraction on formaldehyde forming isocyanic acid (HNCO). The model predicts the formation of 1300 ppm of HNCO which is also not measured. HNCO is the major source of amino radical (NH_2) ultimately producing ammonia. NCO also reacts with NO and NO_2 forming N_2O together with CO and CO_2, respectively. At $T = 925$ K the model predicts the formation of 170 ppm N_2O, rising to 1100 ppm at $T = 1000$ K. According to numerical simulations, the nitrogen balance is closed by the formation of considerable amounts of N_2 (580 ppm at $T = 925$ K, and 4000 ppm at $T = 1000$ K). An additional rate of production analysis at $T = 925$ K focusing specifically on pyrrole consumption is reported in Fig. S13 of SM-1. Revision of the NO_x subset of the CRECK kinetic framework [34] is beyond the aim of this study, but further comprehensive assessments of these competing channels, and also the potential NO_x formation from the N-containing intermediates like NH_3 and HCN are highly recommended. Nevertheless, aiming to explore possible model shortcomings leading to such deviations in NO and NO_2 profiles, we provide a detailed kinetic analysis in Section 5 of SM-1.

Pyridine (C_5H_5N), formamide (CH_3NO), 2-carbonitrile-pyrrole, and 3-carbonitrile-pyrrole (C_4H_4NCN) are also detected, identified, and quantified (see Fig. 4). Peak mole fractions are

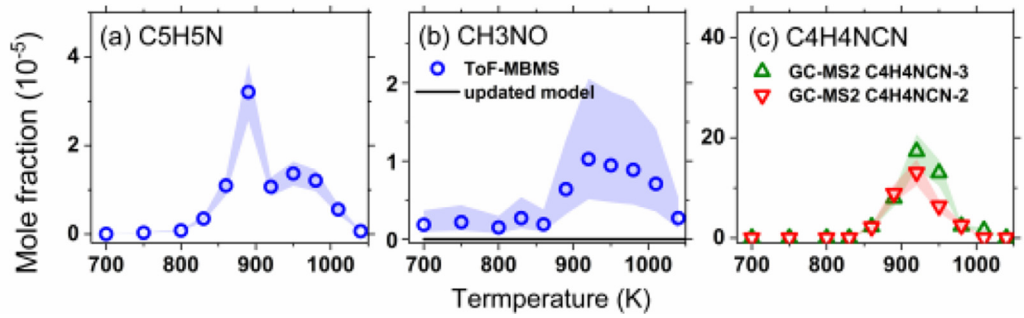

Fig. 4. Mole fraction versus temperature profiles of pyridine (C_5H_5N), formamide (CH_3NO), 2- and 3-carbonitrile-pyrrole (C_4H_4NCN). JSR conditions: fuel concentration 1.05%, φ=0.5, p = 1 bar, τ=2.0 s.

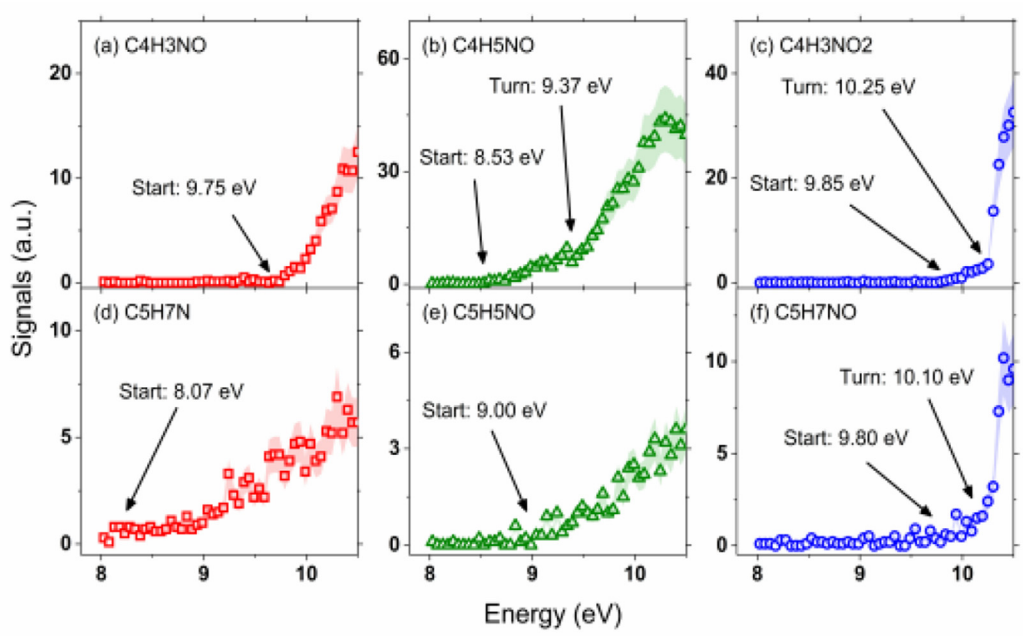

Fig. 5. PIE curve of C_4 and C_5 N-containing species.

30, 10, and 200 ppm, respectively, highlighting the important role of carbonitrile-pyrrole isomers. These N-containing species are missing or under-predicted (CH_3NO in Fig. 4(b)) by both models, pointing at the need for further improving N-containing species formation chemistry. For example, ipso-addition reactions of CN may account for the formation of carbonitrile-pyrrole isomers.

3.2. *Identification of C_4 and C_5 N-containing species*

Other than the quantified species, nine C_4 and C_5 N-containing compounds are newly detected by ToF-MBMS using SVUV as PI source. Except for the aforementioned pyridine and two carbonitrile-pyrrole isomers, Fig. 5 shows the PIE curves for six chemical compositions: C_4H_3NO, C_4H_5NO, $C_4H_3NO_2$, C_5H_7N, C_5H_5NO, and C_5H_7NO. Their signal versus temperature profiles are presented in Fig. 6. An overview of the species signals is presented in the mass spectrum from ToF-MBMS at the energy of 10.50 eV (see Fig. S14 in SM-1).

For the signal profiles of C_4 and C_5 N-containing species, the temperatures of maximum mole fractions (see Fig. 6) appear to be around 900 K. This falls into the temperature region where fuel consumption is underpredicted (900–1000 K), suggesting the possible effects of the missing formation pathways on the fuel reactivity. The combination of measured PIE curves and IE calculations of 28 possible candidates (see Fig. S1 and Table S3) helps to elucidate the potential chemical structures. The starting point of the PIE curve for

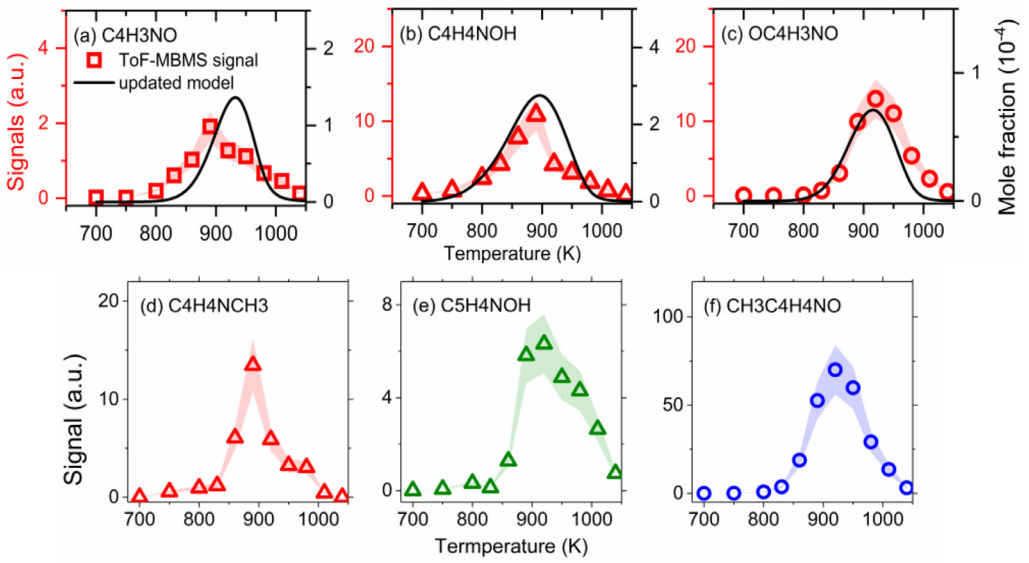

Fig. 6. Signal versus temperature profiles of the unquantified C_4 and C_5 N-containing species (left y-axis). Simulated mole fraction profiles by the updated model for (a) C_4H_3NO, (b) C_4H_5NO, and (c) $C_4H_3NO_2$ are also qualitatively compared in the right y-axis.

C_4H_3NO is 9.75 eV (see Fig. 5(a)), so it is identified as pyrrol-2-one (calculated IE: 9.63 eV). The starting and turning points of the PIE curve for C_4H_5NO are 8.53 eV and 9.37 eV (see Fig. 5(b)), therefore C_4H_5NO is identified as 1,3-dihydro-2H-pyrrol-2-one (calculated IE: 8.50 eV) and 2H-pyrrol-2-ol (calculated IE: 9.46 eV). For $C_4H_3NO_2$, the starting point of the PIE curve is 9.85 eV (see Fig. 5(c)), so it could be 5–hydroxy-pyrrol-2-one (calculated IE: 10.00 eV). The turning point (see Fig. 5(c)) at 10.25 eV might be maleimide (calculated IE: 10.68 eV), which is identified by the GC–MS. The potential structures of C_5 N-containing species are also elucidated: C_5H_7N as methylpyrrole, C_5H_5NO as 2-pyridone, and C_5H_7NO as 5-methyl-2-pyrrolidone. All of the identified structures can be found in Fig. S1 in SM-1. Please note that since many of the potential isomers have close IE, the species identification also depends on the feasible formation pathways of these species in the updated model (see Fig. 7). From the GC–MS measurements, except for $C_4H_3NO_2$, the other C_4 and C_5 N-containing species are not captured. This could be due to their instability in the transfer line or the GC column. The species identification guides the pathway exploration in the following section.

3.3. *Proposed formation pathways and influence on kinetic modeling*

Based on the species identification results, potential formation pathways of C_4 and C_5 N-containing species are proposed in Fig. 7. The entrance channel to the formation of C_4 N-containing intermediates is the addition of OH to pyrrole. The atmospheric oxidation of pyrrole by OH was recently investigated by Mai et al. [35] and re-assessed in this work considering the ring-opening reactions from the OH-addition adduct when solving the multiwell master equation [27]. Due to their importance, the H-atom abstraction reactions from pyrrole by OH, H, CH_3, and HO_2 radicals were also investigated as aforementioned. Calculated energy barriers of H-atom abstraction reactions (details in SM-1, Section 2.3) agree with the values in the literature [35,36] within the expected uncertainties (1–2 kcal/mol). The global OH+C_4H_5N reaction rate, including both H-atom abstractions and addition, agrees with previous experimental measurements [36–38] within a factor of ~1.5 (see Fig. S8 in SM-1). This supports the reliability of the calculations since the addition channel dominates in the reported temperature range (T = 330–450 K).

According to the calculation results, OH addition produces a resonance-stabilized C_4H_5NOH radical (see Fig. 7 and S6 in SM-1) which then undergoes beta-scission to C_4H_4NOH. H-atom abstractions from the hydroxyl group of C_4H_4NOH yield a resonance-stabilized radical (AC_4H_4NO) that may further release the H-atom bonded to nitrogen to form C_4H_3NO. Alternatively, the adduct from OH addition can react with HO_2 and directly produce OH and HOC_4H_5NO, which can lose an H atom through beta-scission to produce OC_4H_4NOH. H-atom abstraction from the tertiary carbon of OC_4H_4NOH yields a resonance-

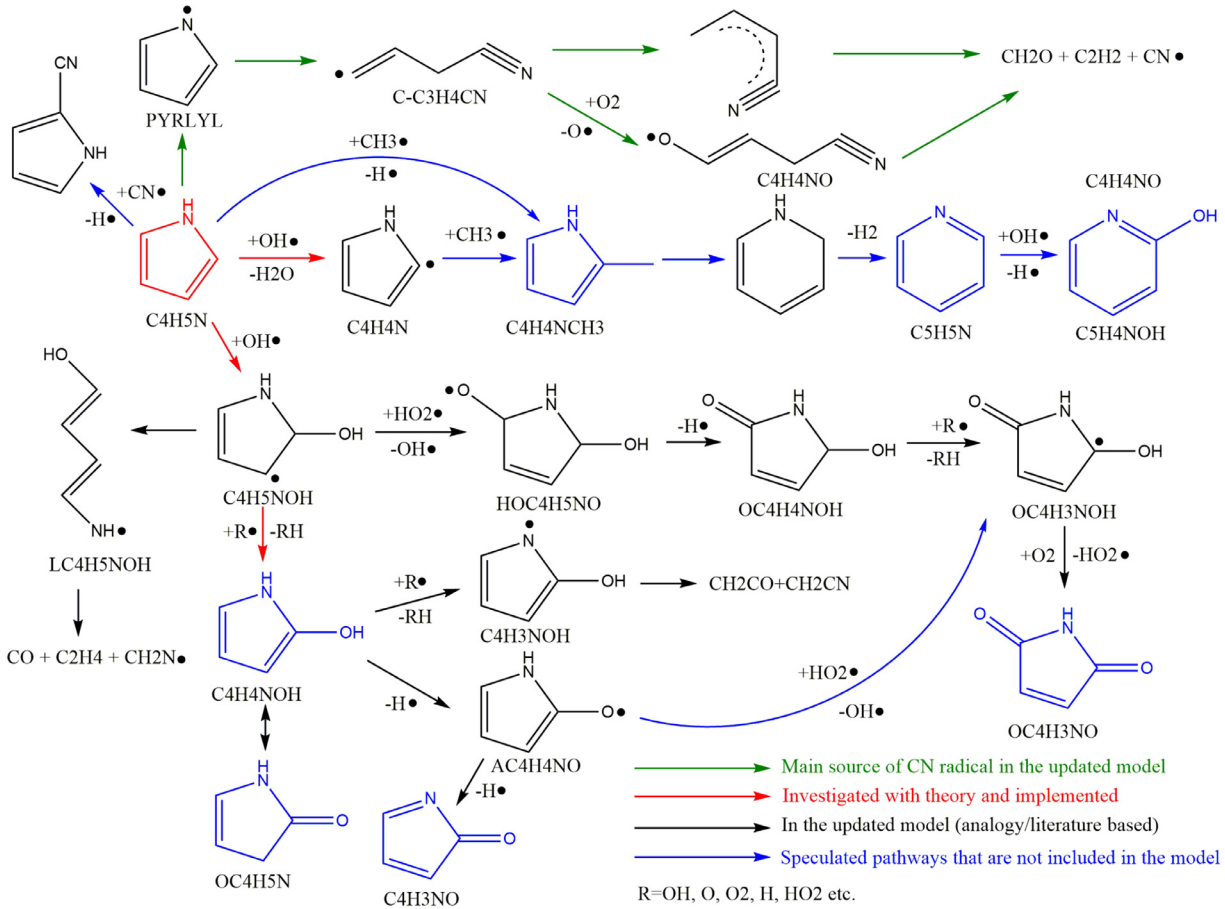

Fig. 7. Proposed formation pathways of C_4 or C_5 N-containing species identified by the experiments. Pyrrole is marked in red, and the identified C_4 and C_5 N-containing molecules are marked in blue.

stabilized OC_4H_3NOH radical that undergoes H-abstraction by O_2 to form OC_4H_3NO (Fig. 7). The rate coefficients for these new reaction pathways that have not been calculated theoretically were preliminarily determined based on the analogy with pyrrole primary reactions (e.g. H-atom abstraction reactions, ring-opening, and decomposition reactions) or with resonance-stabilized radical chemistry (e.g., allyl radical) as implemented in the core subset of the CRECK kinetic model [39,40]. Details on the specific source for rate coefficients are reported in the attached CHEMKIN format file (SM-3).

For C_5 N-containing species, pyridine (C_5H_5N) might be produced from the ring enlargement of 2-methyl-pyrrole ($C_4H_4NCH_3$), a product from CH_3 addition on C_4H_4N or CH_3 ipso-substitution of pyrrole (see Fig. 7). The C_4H_4NCN could be directly formed by an ipso-addition reaction releasing the H atom. Further oxidation of pyridine produces 2-pyridone. These proposed pathways are not included in both the original and the updated models, but they deserve a specific theoretical investigation in future kinetic model development.

Due to the missing PICS, signal profiles of C_4H_3NO, C_4H_4NOH, and OC_4H_3NO are presented and compared with simulated mole fraction profiles to have a qualitative look in Fig. 6. The model with the updated rate coefficients and reaction pathways qualitatively predicts the mole fraction profiles of C_4H_3NO, C_4H_4NOH, and OC_4H_3NO with similar trends to the measured signal profiles (see Fig. 6), although the simulated mole fractions of OC_4H_3NO might be underestimated because of higher signals than that of C_4H_3NO and C_4H_4NOH (see Fig. 6(c)). Furthermore, the updated model improves the fuel consumption profiles (see Fig. 1(a)) as well as the predictions for many hydrocarbons and N-containing species (see Figs. 1 and 2) as aforementioned. However, predictions for some species like ethylene became worse by the updated model, which may need further investigations. The improved model performance indicates the impact of the explored reactions on fuel reactivity and pollutant formation, and motivates further kinetic investigations to gain a better understanding of N-containing pollutant formation from fuel nitrogen. In particular, cyano radical/fuel interaction, ring-enlargement reactions from the addition/recombination of methyl radicals, and secondary reactivity of the OH-addition adduct deserve to be investigated.

4. Conclusions

The oxidation chemistry of pyrrole, an important biomass tar component, is investigated in this work by advanced experimental techniques, theoretical calculations, and kinetic modeling. New insights into the oxidation chemistry of pyrrole are provided. In particular:

1. The use of different experimental techniques not only provides cross examination for each other, but also expands the N-containing species measurements. Furthermore, many C_4 and C_5 N-containing species were newly detected. Their possible structures were identified by the measured PIE curves and calculated IE. The species identification motivates further pathway investigations and indicates targets for model refinement and assessment.
2. Based on the identified species structures, potential formation pathways are proposed with OH addition as the entrance reaction. Important reactions, e.g., H-atom abstractions by H, OH, CH_3, and HO_2 as well as OH addition reactions, were calculated by quantum chemistry at high level of theory.
3. The newly calculated rate coefficients were implemented in the CRECK model. The updated model not only qualitatively captures the signal profiles of newly-identified C_4 N-containing species, but also improves the predictions of fuel reactivity and other species. The improved model performance substantiates the importance of the investigated reactions, and provides further insights into N-containing pollutants formation from fuel nitrogen, motivating further efforts in the fuel-NO_x chemistry.

Declaration of Competing Interest

The authors declare that they have no known competing financial interests or personal relationships that could have appeared to influence the work reported in this paper.

Acknowledgements

BC, CH, KL, and HP acknowledge the financial support by the Deutsche Forschungsgemeinschaft under Germanyś Excellence Strategy – Cluster of Excellence 2186 „The Fuel Science Center" – ID: 390919832. SF and HP acknowledge the support by the Deutsche Forschungsgemeinschaft (DFG, German Research Foundation) within the framework of the collaborative research center SFB/Transregio 129 "Oxyflame". The IE calculation work was supported by the funding from KAUST CRG project under project number URF/1/4688–01–01. The experimental work was supported by Hefei Science Center, CAS(2020HSC-KPRD001 and 2021HSC-UE005). The kinetic model work at Politecnico di Milano was funded by the European Union's Horizon 2020

Research and Innovation Program (Grant Agreement 723706 - IMPROOF Project, H2020-INDCE-2016–17/H2020-SPIRE-S016).

Supplementary materials

Supplementary material associated with this article can be found, in the online version, at doi:10.1016/j.proci.2022.07.019.

References

[1] S. Chu, A. Majumdar, Opportunities and challenges for a sustainable energy future, Nature 488 (2012) 294–303.
[2] P. Glarborg, J.A. Miller, B. Ruscic, S.J. Klippenstein, Modeling nitrogen chemistry in combustion, Prog. Energy Combust. Sci. 67 (2018) 31–68.
[3] M. Hupa, O. Karlström, E. Vainio, Biomass combustion technology development–It is all about chemical details, Proc. Combust. Inst. 36 (2017) 113–134.
[4] P.E.A. Debiagi, M. Trinchera, A. Frassoldati, T. Faravelli, R. Vinu, E. Ranzi, Algae characterization and multistep pyrolysis mechanism, J. Anal. Appl. Pyrolysis 128 (2017) 423–436.
[5] T. Yamamoto, T. Kuwahara, K. Nakaso, T. Yamamoto, Kinetic study of fuel NO formation from pyrrole type nitrogen, Fuel 93 (2012) 213–220.
[6] A. Lifshitz, C. Tamburu, A. Suslensky, Isomerization and decomposition of pyrrole at elevated temperatures: studies with a single-pulse shock tube, J. Phys. Chem. 93 (1989) 5802–5808.
[7] J.C. Mackie, M.B. Colket III, P.F. Nelson, M. Esler, Shock tube pyrolysis of pyrrole and kinetic modeling, Int. J. Chem. Kinet. 23 (1991) 733–760.
[8] X. Hong, L. Zhang, T. Zhang, F. Qi, An experimental and theoretical study of pyrrole pyrolysis with tunable synchrotron VUV photoionization and molecular-beam mass spectrometry, J. Phys. Chem. A 113 (2009) 5397–5405.
[9] F. Dubnikova, A. Lifshitz, Isomerization of pyrrole. Quantum chemical calculations and kinetic modeling, J. Phys. Chem. A 102 (1998) 10880–10888.
[10] L. Zhai, X. Zhou, R. Liu, A theoretical study of pyrolysis mechanisms of pyrrole, J. Phys. Chem. A 103 (1999) 3917–3922.
[11] M. Martoprawiro, G.B. Bacskay, J.C. Mackie, Ab initio quantum chemical and kinetic modeling study of the pyrolysis kinetics of pyrrole, J. Phys. Chem. A 103 (1999) 3923–3934.
[12] G.B. Bacskay, M. Martoprawiro, J.C. Mackie, The thermal decomposition of pyrrole: An ab initio quantum chemical study of the potential energy surface associated with the hydrogen cyanide plus propyne channel, Chem. Phys. Lett. 300 (1999) 321–330.
[13] J. MacNamara, J. Simmie, The high temperature oxidation of pyrrole and pyridine; ignition delay times measured behind reflected shock waves, Combust. Flame 133 (2003) 231–239.
[14] J. Luo, C. Zou, Q. Lin, W. Xia, H. Zou, S. Wang, A shock tube and modeling study on the auto-ignition properties of pyrrole in O2/CO2 atmosphere at elevated pressures, Combust. Flame 230 (2021) 111458.
[15] Z. Tian, Y. Li, T. Zhang, A. Zhu, Z. Cui, F. Qi, An experimental study of low-pressure premixed pyrrole/oxygen/argon flames with tunable synchrotron photoionization, Combust. Flame 151 (2007) 347–365.
[16] M. Lumbreras, M. Alzueta, A. Millera, R. Bilbao, A study of pyrrole oxidation under flow reactor conditions, Combust. Sci. Technol 172 (2001) 123–139.
[17] M. Pelucchi, S. Arunthanayothin, Y. Song, O. Herbinet, A. Stagni, H.-H. Carstensen, T. Faravelli, F. Battin-Leclerc, Pyrolysis and Combustion Chemistry of Pyrrole, a Reference Component for Bio-oil Surrogates: Jet-Stirred Reactor Experiments and Kinetic Modeling, Energy & Fuels 35 (2021) 7265–7284.
[18] Q. Xu, B. Liu, W. Chen, T. Yu, Z. Zhang, C. Zhang, L. Wei, Z. Wang, Comprehensive study of the low-temperature oxidation chemistry by synchrotron photoionization mass spectrometry and gas chromatography, Combust. Flame 236 (2022) 111797.
[19] B. Chen, B.D. Ilies, W. Chen, Q. Xu, Y. Li, L. Xing, J. Yang, L. Wei, N. Hansen, H. Pitsch, Exploring low temperature oxidation of 1-butene in jet-stirred reactors, Combust. Flame 222 (2020) 259–271.
[20] C. Faiola, M. Erickson, V. Fricaud, B. Jobson, T.M. Vanreken, Quantification of biogenic volatile organic compounds with a flame ionization detector using the effective carbon number concept, Atmos. Meas. Tech. 5 (2012) 1911–1923.
[21] C. Huang, B. Yang, F. Zhang, Calculation of the absolute photoionization cross-sections for C1–C4 Criegee intermediates and vinyl hydroperoxides, J. Chem. Phys. 150 (2019) 164305.
[22] K. Moshammer, A.W. Jasper, D.M. Popolan-Vaida, Z. Wang, V.S. Bhavani Shankar, L. Ruwe, C.A. Taatjes, P. Dagaut, N. Hansen, Quantification of the keto-hydroperoxide (HOOCH2OCHO) and other elusive intermediates during low-temperature oxidation of dimethyl ether, J. Phys. Chem. A 120 (2016) 7890–7901.
[23] L.A. Curtiss, P.C. Redfern, K. Raghavachari, Gaussian-4 theory, J. Chem. Phys. 126 (2007) 084108.
[24] J.D. Watts, J. Gauss, R.J. Bartlett, Coupled-cluster methods with noniterative triple excitations for restricted open-shell Hartree–Fock and other general single determinant reference functions. Energies and analytical gradients, J. Chem. Phys. 98 (1993) 8718–8733.
[25] Y. Zhao, D.G. Truhlar, The M06 suite of density functionals for main group thermochemistry, thermochemical kinetics, noncovalent interactions, excited states, and transition elements: two new functionals and systematic testing of four M06-class functionals and 12 other functionals, Theo. Chem. Acc. 120 (2008) 215–241.
[26] C. Cavallotti, M. Pelucchi, Y. Georgievskii, S. Klippenstein, EStokTP: electronic structure to temperature-and pressure-dependent rate constants—a code for automatically predicting the thermal kinetics of reactions, J. Chem. Theo. Comput. 15 (2018) 1122–1145.
[27] Y. Georgievskii, J.A. Miller, M.P. Burke, S.J. Klippenstein, Reformulation and solution of the master equation for multiple-well chemical reactions, J. Phys. Chem. A 117 (2013) 12146–12154.
[28] S.N. Elliott, K.B. Moore III, A.V. Copan, M. Keçeli, C. Cavallotti, Y. Georgievskii, H.F. Schaefer III, S.J. Klippenstein, Automated theoretical chemical

kinetics: Predicting the kinetics for the initial stages of pyrolysis, Proc. Combust. Inst. 38 (2021) 375–384.
[29] L.P. Maffei, M. Pelucchi, C. Cavallotti, A. Bertolino, T. Faravelli, Master equation lumping for multi-well potential energy surfaces: A bridge between ab initio based rate constant calculations and large kinetic mechanisms, Chem. Eng. J. 422 (2021) 129954.
[30] R. Kee, F. Rupley, J. Miller, Chemkin-Pro 15112, Reaction Design, San Diego, CA, USA, 2011.
[31] A. Cuoci, A. Frassoldati, T. Faravelli, E. Ranzi, OpenSMOKE++: An object-oriented framework for the numerical modeling of reactive systems with detailed kinetic mechanisms, Computer Physics Communications 192 (2015) 237–264.
[32] W.L. Oberkampf, M.F. Barone, Measures of agreement between computation and experiment: validation metrics, J. Comput. Phys. 217 (2006) 5–36.
[33] D. Baulch, C.T. Bowman, C. Cobos, R. Cox, Th. Just, JA Kerr, MJ Pilling, D. Stocker, J. Troe, W. Tsang, RW Walker, J. Phys. Chem. Ref. Data 34 (2005) 757–1397.
[34] Y. Song, L. Marrodán, N. Vin, O. Herbinet, E. Assaf, C. Fittschen, A. Stagni, T. Faravelli, M. Alzueta, F. Battin-Leclerc, The sensitizing effects of NO2 and NO on methane low temperature oxidation in a jet stirred reactor, Proc. Combust. Inst. 37 (2019) 667–675.
[35] T.V.-T. Mai, H.T. Nguyen, L.K. Huynh, Ab initio kinetic mechanism of OH-initiated atmospheric oxidation of pyrrole, Chemosphere 263 (2021) 127850.
[36] T.J. Dillon, M.E. Tucceri, K. Dulitz, A. Horowitz, L. Vereecken, J.N. Crowley, Reaction of hydroxyl radicals with C4H5N (pyrrole): temperature and pressure dependent rate coefficients, J. Phys. Chem. A 116 (2012) 6051–6058.
[37] T.J. Wallington, Kinetics of the gas phase reaction of OH radicals with pyrrole and thiophene, Int. J. Chem. Kinet. 18 (1986) 487–496.
[38] F. Witte, C. Zetzsch, Examination of the temperature dependence for the reaction of OH radicals with heterocyclic aromatics (imidazole, furan, pyrrole and thiophene) and the unimolecular decay of the adducts imidazole-OH and thiophene-OH, 9th Int Symp on Gas Kinetics (1986) 20-25.
[39] S.M. Burke, W. Metcalfe, O. Herbinet, F. Battin-Leclerc, F.M. Haas, J. Santner, F.L. Dryer, H.J. Curran, An experimental and modeling study of propene oxidation. Part 1: Speciation measurements in jet–stirred and flow reactors, Combust. Flame 161 (2014) 2765–2784.
[40] C.F. Goldsmith, S.J. Klippenstein, W.H. Green, Theoretical rate coefficients for allyl+ HO2 and allyloxy decomposition, Proc. Combust. Inst. 33 (2011) 273–282.